Photoelectron determination of the attenuation of low-energy electrons in Al_2O_3

F. L. Battye, J. G. Jenkin, J. Liesegang, and R.C.G. Leckey
Physics Department, La Trobe University, Bundoora, Victoria, Australia 3083
(Received 5 October 1973)

The attenuation length for electrons in Al_2O_3 has been determined to vary from 6.7 Å at 157 eV to 16.7 Å at 1404 eV by means of an x-ray-photoelectron spectroscopic technique. The attenuation of photoelectron and Auger-electron lines from a substrate was monitored as the thickness of an overlayer of Al_2O_3 was increased, the results being corrected for the asymmetry of photoelectron angular distributions from various subshells and for effects due to the geometry of the spectrometer. The results have been compared with a number of theoretical models of electron scattering. The major energy-loss process has been demonstrated to be due to inelastic scattering involving valence-band electrons.

I. INTRODUCTION

An accurate knowledge of the attenuation length for electrons in solids with energies in the range 0.15–1.5 keV is of the utmost importance in the quantitative interpretation of a wide range of electron spectroscopic measurements. This is the energy range of interest in x-ray-photoelectron spectroscopy, for example, and many Auger transitions also result in the emission of electrons with kinetic energies of this order. The scarcity of reliable measurements of attenuation lengths for such low-energy electrons is directly attributable to the shortness of the attenuation length, which is typically 15 Å or less in this energy region.[1]

We report here, by means of a technique which directly monitors the attenuation of photoelectrons, the determination of the energy dependence of the attenuation length of electrons in Al_2O_3 covering the energy range 150–1400 eV. The results so obtained are compared with the predictions of two theoretical models: one in which all energy states in Al_2O_3 (including the valence band) are considered to be tightly bound, and the other extreme situation in which the valence-band electrons are considered to be free.

II. EXPERIMENTAL METHOD

A. General

Some measurements of attenuation lengths in solids have recently been made by an Auger-electron spectroscopic technique[2–5] which monitors the attenuation of substrate Auger signals as the thickness of a thin covering film of some dissimilar material is increased (or, alternatively, the increase in an Auger signal characteristic of the thin film is monitored). Such measurements suffer from the serious disadvantage that the primary electron beam which is used to cause inner-shell ionization, which then leads to Auger recombination, must itself be scattered and attenuated by the presence of the thin film. This effect can clearly not be eradicated without prior knowledge of the attenuation length for electrons of energy equal to that of the primary beam.

The use of an x-ray-photon beam as the primary probe obviates this difficulty because of the very much larger attenuation length for x-ray photons than for electrons of similar energies,[6] and because the mass-absorption coefficients for soft-x-ray photons are generally well known. By suitable choice of photon energy and substrate material, photoelectrons and photo-Auger electrons of well-defined energies may be generated over a wide energy range; and by monitoring the attenuation of such electrons in their passage through a thin film of some dissimilar material which is essentially transparent to the incident photon beam, an inelastic mean free path (λ) or attenuation length for electrons of each energy may be obtained from the relation

$$I = I_0 e^{-t/\lambda}, \tag{1}$$

where I and I_0 represent the intensity of a particular electron line with and without a covering thin film of thickness t.

The x-ray-photoelectron spectrometer used in this work is shown schematically in Fig. 1 and is described in some detail in Refs. 7 and 8. In order to obtain high photoelectron luminosity the x-ray source and sample rod are of cylindrical symmetry, with electrons emitted from the sample into a cone of half-angle 45° ± 2° being accepted into the spherical-sector electrostatic energy analyzer. The use of this particular geometry is advantageous in terms of over-all spectrometer sensitivity and signal-to-noise ratio, but leads to a number of complications for the purposes of the present experiment. The use of a cylindrical sample rod poses certain difficulties in the controlled evaporation of very thin and uniform films (see Sec. IIB) and, in addition, results in the sample being irradiated by x rays at a variety of angles of incidence and in the emission of electrons over a range of angles of emergence which are still within the angular acceptance of the energy analyzer. These

latter considerations are, however, capable of straightforward analytical treatment as given in Sec. IIC.

After energy analysis, electrons are detected by a Cu-Be dynode electron multiplier (EMI type 9643/2B) and the data acquired in a Nuclear Data 1024-channel multiscalar whose channel-advance mechanism is synchronized with the scan voltage of the spectrometer.

B. Preparation and control of thin-film parameters

In order to deposit a uniformly thick film for either substrate or sample overlayer purposes, the cylindrical sample rod could be raised from the measurement position (as shown in Fig. 1) and rotated about a horizontal symmetry axis, approximately 20 cm above a pair of evaporation boats. In close proximity to the sample when in this position, a quartz-crystal-detector head was positioned in order to monitor and control automatically the rate of deposition by means of an Ultek thin-film deposition system[9] which was coupled to the power source driving the evaporation boat in use. By rotating the sample rod at a constant rate and operating the evaporation system at a constant evaporation rate, a uniform film of thickness t could be deposited on the sample rod of radius a. This technique is essentially that used previously by Steinhardt *et al.*[10] A Varian Å-scope (multiple-beam interferometer) with an accuracy of ± 25 Å for films of thickness > 200 Å was used for the calibration of the quartz-crystal oscillator by means of a series of controlled evaporations. We estimate that the average thickness of each of the films used in the present work has been determined to an accuracy of ± 2%. Because the pressure in the sample preparation area of the spectrometer rose to ~ 1×10^{-6} torr during evaporation, the evaporation of 99.999%-pure Al at a rate of 0.25 Å per second resulted in the deposition of completely oxidized films as observed by Klasson *et al.*[11]

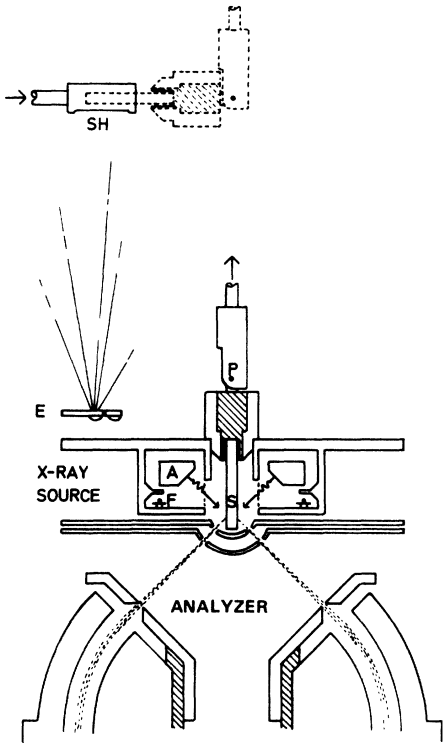

FIG. 1. Sample preparation area and part of the spectrometer. Positions of sample (S) are shown both for measurement and for evaporation. The cylindrical shield (SH) encloses the sample during evaporation from one of two evaporation boats (E) and is equipped with a shutter. (A is anode; F is filament.)

Films of Al_2O_3 were produced with thicknesses in the range 5–30 Å (i.e., of the order of an electron attenuation length at the energies of interest) and consequently it was important to ensure that no islanding or other irregular deposition patterns were present. Sample films of Al_2O_3 were examined with this in mind in a scanning electron microscope (SEM) equipped with an energy-dispersive x-ray detector.[12] Although the surface topography of the sample was clearly seen to be complex the distribution of Al over the sample surface was observed to be essentially isotropic as seen by the detection of Al $K\alpha$ radiation caused by the incident electron beam in the SEM. From this evidence, and from the evidence of results to be discussed later, we are satisfied that the thin films used here were uniform and of constant thickness.

C. Geometrical corrections

As mentioned earlier, because of the geometry of the spectrometer shown in Fig. 1, x rays are incident on the cylindrical sample rod at a variety of angles ϕ (Fig. 2). Although the attenuation of the x rays used in this work is very small, a complete mathematical treatment must include this effect, which will clearly be different for different angles of incidence ϕ. We consequently define an attenuation length λ_γ for x rays entering the substrate, and ignoring surface and interface refraction, we relate the x-ray flux per second in an element of the substrate to the incident x-ray flux per second $\delta\Phi_\gamma(0)$ emitted from a small element of anode surface via

$$\delta\Phi_\gamma \approx \delta\Phi_\gamma(0)\exp[-\sqrt{2}\,(a-r)/\lambda_\gamma\cos(\eta-\kappa)], \qquad (2)$$

where the azimuthal angle of the substrate volume element is κ and that of the anode surface element is approximately η. Since a is experimentally much smaller than the x-ray-anode radius and the spectrometer-entrance-slit radius, the polar angles of $\hat{k}_\gamma$ and $\hat{k}_e$ are taken always to be $\pi/4$ (see Fig. 2).

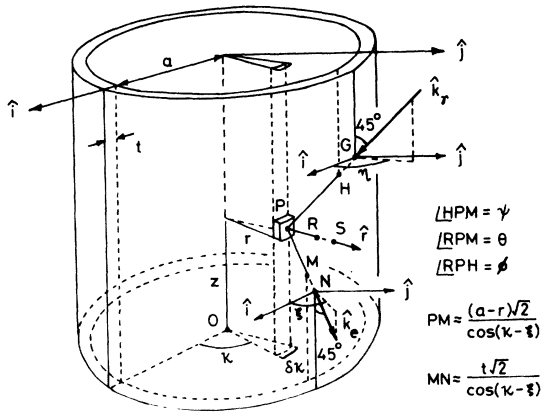

FIG. 2. Geometrical arrangement of x-ray source, sample, and spectrometer. The small volume element of substrate ($r\,\delta r\,\delta z\,\delta\kappa$) at the point P is irradiated by x rays of wave vector $\vec{k}_\gamma$ and emits electrons of wave vector $\vec{k}_e$.

Thus the number of photoeclectrons per second (δI) which are produced within an element of substrate (of volume $\delta A\,\delta r$ located $a-r$ from the surface) by photons incident at an angle ϕ, and which are emitted into a solid angle $\delta\Omega$ at θ to the substrate normal (Fig. 2), is

$$\delta I = \delta\Phi_\gamma \cos\phi \frac{d\sigma}{d\Omega} N\,\delta r\,\delta\Omega\,\delta A, \tag{3}$$

where N is the atomic density of the substrate and $d\sigma/d\Omega$ is the differential photoelectron cross section of the relevant subshell for photons of energy $h\nu$. If an overlayer of dissimilar material covers the substrate this will cause an additional x-ray attenuation given by $\exp[-\sqrt{2}t/\lambda_\gamma'\cos(\eta-\kappa)]$ if the overlayer has a photon attenuation length described by λ_γ'.

The photoelectrons so generated within a small element of substrate will be emitted at a variety of angles to the direction of the incident-photon wave vector depending on the atomic shell from which they are ejected. Since this angular distribution determines the path length in the sample which electrons must travel before reaching the surface, it is essential that this factor be incorporated in the theoretical interpretation. The differential cross section may then be written[13]

$$\frac{d\sigma}{d\Omega} = \frac{\sigma}{4\pi}[(1-\tfrac{1}{2}\beta)+\tfrac{3}{4}\beta\sin^2\psi(\eta,\xi)], \tag{4}$$

where ψ is the angle between the incoming x-ray direction $\hat{k}_\gamma$ and the direction of the photoemitted electron $\hat{k}_e$, β is the asymmetry parameter, and σ is the relevant total subshell photoelectron cross section. The angle ψ is a function both of the x-ray azimuthal direction angle ($\approx\eta$) and the azimuthal angle for the emitted photoelectron ($\approx\xi$). From Refs. 13–15 we have that

$\beta = 2.0$ for s shells

$= 1.0 \to 1.5$ for p shells

$= 1.5$ for $d_{5/2}$ shells

$= 1.2$ for $f_{7/2}$ shells,

whereas for an isotropic distribution, as may be assumed for Auger-electron emission, $\beta = 0$.

We assume that the photoelectrons are attenuated in the substrate according to the factor

$$\exp[-\sqrt{2}(a-r)/\lambda_e\cos(\kappa-\xi)], \tag{5}$$

with the corresponding factor

$$\exp[-\sqrt{2}t/\lambda_e'\cos(\kappa-\xi)] \tag{6}$$

in the overlayer, λ_e and λ_e' being the electron attenuation lengths in substrate and overlayer, respectively, and θ the angle of emergence of the photoelectron from the sample element with respect to the element normal.

We may thus write that the intensity of photoelectrons, due to photon flux $\delta\phi_\gamma(0)(\propto\delta\eta)$, which emerge at angle θ into solid angle $\delta\Omega$ ($\propto\delta\xi$) from the substrate element which is $a-r$ below the surface of the overlayer is

$$\begin{aligned}\delta\Upsilon \equiv{}& \frac{\delta I}{\delta A}\\ \propto{}& \cos\phi\exp[-\sqrt{2}(a-r)/\lambda_\gamma\cos(\eta-\kappa)]\\ &\times\exp[-\sqrt{2}t/\lambda_\gamma'\cos(\eta-\kappa)]\exp[-\sqrt{2}(a-r)/\\ &\lambda_e\cos(\kappa-\xi)]\\ &\times\exp[-\sqrt{2}t/\lambda_e'\cos(\kappa-\xi)]\frac{d\sigma}{d\Omega}\delta\eta\,\delta\xi\,\delta r\,.\end{aligned} \tag{7}$$

The total number of photoelectrons emerging per second from the sample and entering the spectrometer is thus obtained by integrating over r and the angles η and ξ. It should be noted (i) that the integrand is essentially constant over the width of the entrance aperture of the spectrometer and (ii) that Eq. (7) suffers no loss of generality by assuming the element in Fig. 2 has $\kappa = 0$.

In evaluating the integral it may be seen from Fig. 2 that the angles θ, ϕ, and ψ are related to the angles κ, η, and ξ through the following relationships:

$$\hat{r} = (\cos\kappa,\ \sin\kappa,\ 0), \tag{8}$$

$$\hat{k}_\gamma \simeq (-\cos\eta,\ -\sin\eta,\ -1)/\sqrt{2}, \tag{9}$$

$$\hat{k}_e \simeq (\cos\xi,\ \sin\xi,\ -1)/\sqrt{2}, \tag{10}$$

whence

$$\cos\psi = \hat{k}_e\cdot\hat{k}_\gamma \simeq [1-\cos(\eta-\xi)]/2, \tag{11}$$

$$\cos\phi = -\hat{k}_\gamma\cdot\hat{r} \simeq \cos(\eta-\kappa)/\sqrt{2}, \tag{12}$$

$$\cos\theta = \hat{k}_e \cdot \hat{r} \simeq \cos(\xi - \kappa)/\sqrt{2}. \quad (13)$$

The anisotropic factor in Eq. (4) may then be rearranged so that

$$\frac{d\sigma}{d\Omega} = \frac{\sigma}{4\pi}\{1 + [1 + 6\cos(\xi - \eta) - 3\cos^2(\xi - \eta)]\beta/16\} \quad (14)$$

and the observed photoelectron intensity as obtained by integration of Eq. (7) then becomes

$$\Upsilon \propto \int_{-\pi/2}^{\pi/2}\int_{-\pi/2}^{\pi/2}\int_0^a \exp[\sqrt{2}(r-a)(1/\lambda_\gamma\cos\eta + 1/\lambda_e\cos\xi)] \times \exp[-\sqrt{2}t(1/\lambda_\gamma + 1/\lambda_\gamma')/\cos\eta + 1/\lambda_e'\cos\xi] \times\{1 + [1 + 6\cos(\xi-\eta) - 3\cos^2(\xi-\eta)]\beta/16\} \times \cos\eta\, dr\, d\eta\, d\xi. \quad (15)$$

In the present experiment we make the following assumption concerning the magnitudes of the mean free paths: $\lambda_\gamma \sim \lambda_\gamma' \gg \lambda_e$, λ_e'. Integration over r and η then yields

$$\Upsilon \propto \int_0^{\pi/2}\exp[-\sqrt{2}t/\lambda_e'\cos\xi][2 - (1 + \cos 2\xi - 3\pi\cos\xi)\beta/16]\cos\xi\, d\xi. \quad (16)$$

This integral has been numerically evaluated for $-\pi/2 \leq \xi \leq \pi/2$, but because of the exponential term, the effective range of ξ is actually much less. The result may be compared with the rudimentary form of the attenuation law, Eq. (1), which assumes that all photoelectrons leave the sample at $\theta = \pi/4$, i.e., $\xi = 0$. As may be seen in Fig. 3, the effect of the photoemission angular asymmetry parameter β is clearly small but the correction which allows for the geometry of the spectrometer is significant.

III. EXPERIMENTAL RESULTS

The applicability of Eq. (16) is illustrated in Fig. 4 which shows the attenuation of the $4f_{7/2}$ level from a gold substrate illuminated by Al $K\alpha$ photons, as a function of the overlayer (Al_2O_3) thickness t. Representative spectra of the $Au_{7/2,5/2}$ doublet are included to illustrate the signal-to-noise ratio achieved.

Gold, copper, and germanium substrates were employed in the present work, together with Al $K\alpha$ (1487 eV) and C $K\alpha$ (277 eV) x rays, as indicated in Table I, which also lists the numerical values of the attenuation lengths. The attenuation lengths were obtained by adjusting the value of λ_e' in Eq. (16) so as to match the experimental data in the manner illustrated by Fig. 4 for the particular case of the Au $4f_{7/2}$ peak.

Results for the attenuation length of 150–1500-eV electrons in Al_2O_3 are displayed in Fig. 5, which also includes data by Klasson *et al.* for 1389 and 2856 eV,[11] Gesell and Arakawa for 20 eV,[16] and Kanter[17] at 5, 1500, and 2000 eV. Kanter's results and those of Gesell and Arakawa refer to largely unoxidized samples of Al. The present results are significant in that they extend previous measurements into the region between 100 and 1 keV, which is of particular interest for the interpretation of many current electron-spectroscopic measurements.

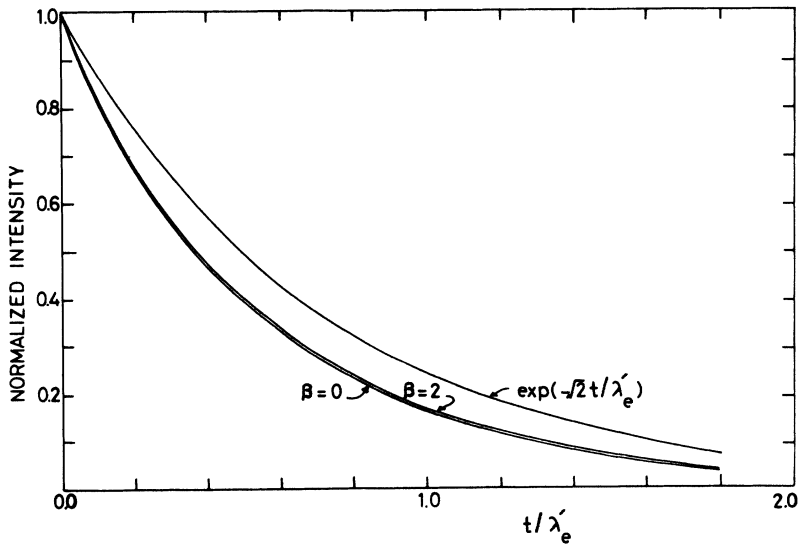

FIG. 3. Attenuation of electron intensity by covering films of relative thickness t/λ_e' as given by Eq. (16) for the cases $\beta = 0$ and $\beta = 2$, and as given by the rudimentary form $I \sim e^{-\sqrt{2}t/\lambda_e'}$.

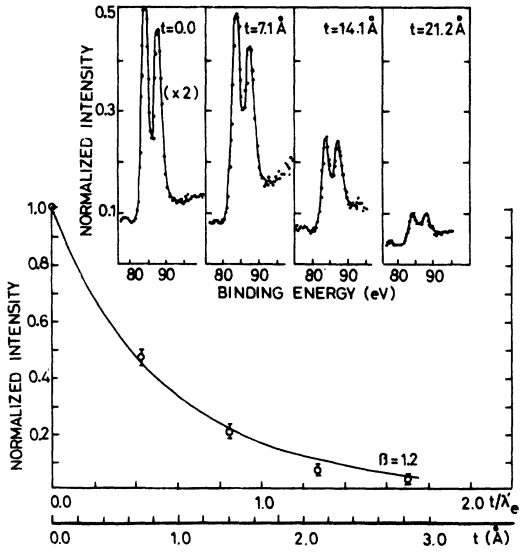

FIG. 4. Data from attenuation of the Au $4f_{7/2}$ photoelectron peak by Al_2O_3 films of thickness t fitted to the curve of attenuation vs relative thickness t/λ_e' from Eq. (16) for the case $\beta = 1.2$.

IV. THEORETICAL CONSIDERATIONS

A theoretical treatment of electron scattering in solids at these energies is fraught with difficulties. We have, however, attempted to delineate the problem by calculating the attenuation lengths to be expected on the basis of some extreme theoretical assumptions.

A. Tight-binding model

The most important scattering mechanisms for fast photoelectrons as they traverse an Al_2O_3 sample towards the surface are likely to be inner-shell ionizations and individual scattering events involving a valence-band electron. For the particular case of Al_2O_3 we have chosen to ignore the possibility of collective interactions with valence-band electrons (plasmon generation) and have considered phonon collisions to be insignificant as an energy-loss mechanism.

Inner-shell ionization may be treated with some degree of accuracy by means of a scheme introduced by Lotz[18] wherein the Bethe inelastic scattering cross-section formula[19] is modified to include an empirical correction factor which is significant for low-energy incident electrons. Lotz's method, as detailed by Pessa and Newell,[20] also allows for a relativistic correction term to be incorporated which is, however, of no significance in the present work.

Following Pessa and Newell we may thus write the inelastic collision cross section, for electrons of incident energy E_0 interacting with a system possessing a number of inner-core energy levels labeled by the subscript i, as

$$\sigma_{TB} = \sum_i a_i q_i [1 - b_i e^{-c_i E_0/E_i}] \ln(E_0/E_i)/E_0 E_i , \quad (17)$$

where we assume $E_0 \geq E_i$, q_i is the number of electrons in the ith subshell and the constants a_i, b_i, and c_i have been determined by Lotz and are given in the article by Pessa and Newell. In the interests of clarity, the small relativistic correction terms applicable here have been omitted from Eq. (17).

The major difficulty in calculating a total inelastic collision cross section concerns the method to be used in treating collisions involving the valence-band electrons. Such interactions constitute the most probable energy-loss mechanisms, as may be inferred from the fact that the contribution to the cross section from all inner-shell ionizations calculated on the basis of the formula discussed above is an amount ranging from 4% at $E_0 = 100$ eV to 14% at $E_0 = 1500$ eV.

One extreme theoretical assumption consists of taking the view that the Lotz tight-binding formalism may also be applied to the valence-band electrons. It is clear that such a treatment is most likely to be relevant for the lowest-energy incident electrons for which the small binding energy of the valence-band electrons will be of most significance. It is unlikely that this approximation will remain valid for even moderately energetic incident electrons. In order to test this assumption we have applied Eq. (17) (including relativistic correction terms) to all the energy states of Al_2O_3 and have derived an estimate of the energy dependence of the total inelastic mean free path λ_{TB} in this tight-binding approximation from σ_{TB} via

$$\lambda_{TB} = 1/[N_m \sigma_{TB}(Al_2O_3)], \quad (18)$$

where $\sigma_{TB}(Al_2O_3) = 2\sigma_{TB}(Al) + 3\sigma_{TB}(O)$ and where N_m is the molecular density of Al_2O_3.

The result of this calculation is displayed as curve 1 in Fig. 5. The agreement may be seen to be good for energies less than about 250 eV, which is approximately 20 times the average binding energy

TABLE I. Values of the electron attenuation length in Al_2O_3 for energies in the range 150–1400 eV.

X Ray	X-ray energy (eV)	Substrate level	Binding energy (eV)	Electron kinetic energy (eV)	Mean free path (Å)
Al $K\alpha$	1486.7	Au $4f_{7/2}$	83	1404	16.7 ± 0.6
		Au $4d_{5/2}$	334	1153	14.9 ± 0.6
		Cu KLL Auger	···	914	12.9 ± 1.0
		Cu $2p_{3/2}$	931	556	10.1 ± 0.9
		Ge $2p_{3/2}$	1217	270	8.5 ± 1.5
C $K\alpha$	277	Cu $3s_{1/2}$	120	157	6.7 ± 0.5

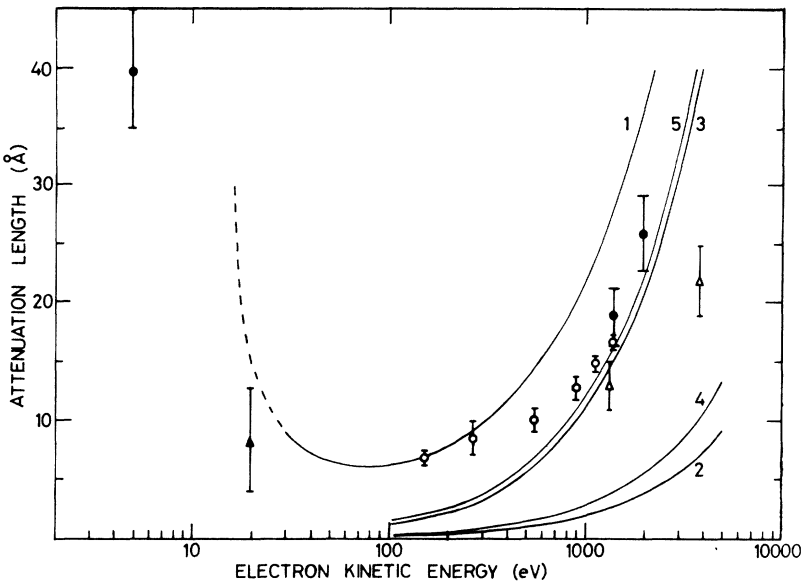

FIG. 5. Attenuation lengths for electrons in Al_2O_3 from the present work (○) together with results of Klasson *et al.* (△). The results of Gesell and Arakawa (▲) and of Kanter (●) for electron attenuation in Al are also shown. Solid lines represent attenuation lengths calculated from 1, the Lotz equation, and 2 and 3, the Mott formalism with minimum allowed energy losses of 1 and 6.3 eV, respectively. Curves labeled 4 and 5 have been derived using a screened-Coulomb-interaction mechanism with minimum energy loss set at 1 and 6.3 eV, respectively.

of valence-band electrons, but the application of this model clearly underestimates the inelastic collision cross section for energies higher than 250 eV.

B. Mott scattering model

At the other extreme we may investigate the results of the assumption that the valence-band electrons in Al_2O_3 are entirely free. One well-known model applicable to this situation is that of Mott scattering, which treats the elastic scattering of identical spin-$\frac{1}{2}$ particles within the framework of a phase-shift analysis.[21] Thus

$$d\sigma_v^{\text{Mott}} = \left(\frac{\zeta^2}{E_0^2}\right)\left(\frac{1}{\sin^4(\frac{1}{2}\theta)} + \frac{1}{\cos^4(\frac{1}{2}\theta)} - \frac{2\cos\{\zeta \ln[\tan^2(\frac{1}{2}\theta)]\}}{\sin^2(\frac{1}{2}\theta)\cos^2(\frac{1}{2}\theta)}\right)d\Omega, \tag{19}$$

where $\zeta = e^2/16\pi\epsilon_0$. A calculation of the mean free path for electrons in Al_2O_3 using Eq. (19) for all valence electrons and Eq. (17) for all other energy levels results in curve 2 shown in Fig. 5, which clearly overestimates the magnitude of the total inelastic collision cross section at all energies of interest. This overestimate is due to the use of an unscreened Coulomb interaction potential implicit in the Mott formalism, which results in the prediction of large numbers of small-angle (small-energy-loss) collisions. It seems likely that the basic Mott model may be improved by the introduction of a minimum energy loss (6.3 eV, being the band gap in Al_2O_3) and by the use of a screened Coulomb interaction potential. As a first step, the prediction of the Mott formula whenever a minimum energy loss of 6.3 eV is imposed is shown in Fig. 5 as curve 3. The agreement with experiment is seen to be considerably improved over that obtained using the basic Mott formalism.

C. Screened-Coulomb-potential model

In the first Born approximation the scattering amplitude A_{ba} for a particle of mass μ to be excited from state ϕ_a to state ϕ_b due to an interaction describable via a potential V is[22]

$$A_{ba} = (-\mu/2\pi\hbar^2) \langle \phi_b | V | \phi_a \rangle \tag{20}$$

which reduces to

$$A_{ba} = (-\mu/2\pi\hbar^2) V(\vec{k}_b - \vec{k}_a) \tag{21}$$

in the plane-wave approximation. For elastic scattering $|\vec{k}_a| = |\vec{k}_b| = |\vec{k}_0|$ and $|\vec{k}_b - \vec{k}_a| = 2k_0 \sin(\frac{1}{2}\theta)$, where θ is the scattering angle. Using a screened interaction potential of the form

$$V(r) = (e^2/4\pi\epsilon_0 r)\, e^{-r/r_0}, \tag{22}$$

where r_0 is a screening radius, it follows that

$$A_{ba}(\theta) = -4e^2/\{16\pi\epsilon_0 E_0[4\sin^2(\tfrac{1}{2}\theta) + 1/k_0^2 r_0^2]\}. \tag{23}$$

Allowing for the spin states of the interacting system we find that

$$d\sigma_v^{\text{SC}} = A(\theta)^2 + A(\pi-\theta)^2 - A(\theta)A(\pi-\theta) = \left(\frac{\zeta^2}{E_0^2}\right)\left[\left(\frac{4}{4\sin^2(\frac{1}{2}\theta) + (k_0 r_0)^{-2}}\right)^2 + \left(\frac{4}{4\cos^2(\frac{1}{2}\theta) + (k_0 r_0)^{-2}}\right)^2 - \frac{16}{[4\sin^2(\frac{1}{2}\theta) + (k_0 r_0)^{-2}][4\cos^2(\frac{1}{2}\theta) + (k_0 r_0)^{-2}]}\right] d\Omega, \tag{24}$$

where $\zeta = e^2/16\pi\epsilon_0$ as before and $\hbar^2 k_0^2 = 2\mu E_0$.

For the present purposes, the screening radius

r_0 has been determined using a formula which is known to be reliable for the description of plasmon generation in simple metals[23]

$$k_0 = (\Delta E/E_F)k_F , \tag{25}$$

where $k_0 = 2\pi/r_0$, k_F is the wave vector of an electron at the Fermi energy E_F, and ΔE is the plasmon energy. Although Eq. (25) is of uncertain validity for the case of Al_2O_3, a characteristic energy loss of approximately 20 eV has been observed in this material and identified as due to plasmon creation.[24] The value of r_0 obtained in this manner is $\simeq 3$ Å.

The results of calculating a mean-free-path function via Eq. (24) is indicated in Fig. 5 as curve 4, where the minimum energy loss has been taken as 1 eV to allow for instrumental resolution. If the minimum energy loss is taken equal to the band gap in Al_2O_3 (6.3 eV), this prediction becomes curve 5. In all cases the inner-core levels have been treated as before via the Lotz method.

V. CONCLUSIONS

Precision measurements of the variation in the total inelastic scattering mean free path for electrons in Al_2O_3 have been made covering the important energy range 150–1500 eV by a photoelectron spectroscopic technique. It has been demonstrated that the major process contributing to the stopping power of Al_2O_3 for such electrons is connected with collisions involving valence-band electrons, and a variety of theoretical models have been investigated in an attempt to describe these collision processes. A model in which the valence electrons are treated as if they were tightly bound has been shown to give reasonable agreement with experiment for electron energies ≤ 250 eV but to be a poor approximation at higher energies. Imposing a minimum-energy-loss condition on free-free collision models, thereby accounting for the band gap in Al_2O_3, has been demonstrated to give good agreement at higher energies. We consider that the agreement between the Mott scattering model and experiment is somewhat fortuitous, being the result of the introduction of the minimum-energy-loss condition, which is equivalent to a truncation of the unscreened Coulomb potential used in this model. The introduction of such a minimum energy loss would not be possible in the treatment of a metal for which the Mott formula would clearly overestimate the collision cross section. Despite some uncertainty in the value to be used for the screening parameter r_0 in the screened Coulomb model we consider this model to represent a reasonable treatment of electron scattering for energies in the region 1–5 keV in Al_2O_3.

[1]E. Bauer, Vacuum 22, 539 (1972).
[2]M. P. Seah, Surf. Sci. 32, 703 (1972).
[3]K. Jacobi and J. Holzl, Surf. Sci. 26, 54 (1971).
[4]J. W. T. Ridgeway and D. Haneman, Surf. Sci. 24, 451 (1971).
[5]D. W. Palmberg and T. W. Rhodin, J. Appl. Phys. 39, 2425 (1968).
[6]B. L. Henke, R. L. Elgin, R. E. Lent, and R. B. Ledingham, Norelco Reporter 14, 112 (1967).
[7]P. C. Kemeny, A. D. McLachlan, F. L. Battye, R. T. Poole, R. C. G. Leckey, J. Liesegang, and J. G. Jenkin, Rev. Sci. Instrum. 44, 1197 (1973).
[8]A. D. McLachlan, R. C. G. Leckey, J. G. Jenkin, and J. Liesegang, Rev. Sci. Instrum. 44, 873 (1973).
[9]Ultek model 60-915, deposit thickness monitor, Ultek model 60-925, deposit rate control, and Ultek model 60-940, power controller.
[10]R. G. Steinhardt, J. Hudis, and M. L. Perlman, Phys. Rev. B 5, 1016 (1972).
[11]M. Klasson, J. Hedman, A. Berndtsson, R. Nilsson, C. Nordling, and D. Melnik, Phys. Scr. 5, 93 (1972).
[12]J. E. O. L. scanning electron microscope, model JSM-U3; Nuclear Diodes EDAX, model 505.
[13]J. W. Cooper and S. T. Manson, Phys. Rev. 177, 157 (1969).
[14]S. T. Manson, J. Electron. Spectrosc. Related Phenomena 1, 413 (1972–3).
[15]M. O. Krause, Phys. Rev. 177, 151 (1969).
[16]T. F. Gesell and E. T. Arakawa, Phys. Rev. Lett. 26, 377 (1971).
[17]H. Kanter, Phys. Rev. B 1, 523 (1970); 1, 2357 (1970).
[18]W. Lotz, Z. Phys. 206, 205 (1967).
[19]H. Bethe, Ann. Phys. (Leipz.) 5, 325 (1930).
[20]V. M. Pessa and W. R. Newell, Phys. Scr. 3, 165 (1971).
[21]A. S. Davydov, *Quantum Mechanics* (Pergamon, New York, 1965), p. 407.
[22]See Ref. 21, p. 376.
[23]H. Raether, in *Springer Tracts in Modern Physics*, edited by G. Höhler (Springer, Berlin, 1965), Vol. 38, pp. 84–157.
[24]M. Suleman and E. B. Pattinson, J. Phys. F 1, L21 (1971).